

Fullerene-encapsulated Cyclic Ozone for the Next Generation of Nano-sized Propellants via Quantum Computation

Thomas W. Watts,¹ Matthew Otten,² Jason T. Necaise,³ Nam Nguyen,⁴ Benjamin Link,⁵ Kristen S. Williams,⁶ Yuval R. Sanders,⁷ Samuel J. Elman,⁷ Maria Kieferova,⁷ Michael J. Bremner,^{8,7} Kaitlyn J. Morrell,⁹ Justin E. Elenewski,⁹ Samuel D. Johnson,¹ Luke Mathieson,⁷ Kevin M. Obenland,⁹ Rashmi Sundareswara,¹ and Adam Holmes¹

¹*HRL Laboratories, LLC, Malibu, CA, USA*

²*Department of Physics, University of Wisconsin – Madison, Madison, WI, USA*

³*Dartmouth College, Hanover, NH, USA*

⁴*Applied Mathematics, Boeing Research & Technology, Huntington Beach, CA, USA*

⁵*Applied Mathematics, Boeing Research & Technology, Orlando, FL, USA*

⁶*Applied Mathematics, Boeing Research & Technology, Huntsville, AL, USA*

⁷*Centre for Quantum Software and Information, School of Computer Science,*

Faculty of Engineering & Information Technology,

University of Technology Sydney, NSW 2007, Australia

⁸*Centre for Quantum Computation and Communication Technology,*

University of Technology Sydney, NSW 2007, Australia

⁹*MIT Lincoln Laboratory, Lexington, MA, USA*

Cyclic ozone additives have the potential to markedly increase the specific impulse of rocket fuel. This would translate to greater efficiency and reduced costs for space lift, granting up to 33% more payload per rocket. While practical efforts to capture this isomer have been unsuccessful, it is possible that cyclic ozone would be stabilized in confined geometries. The required synthetic methods are nonetheless difficult to design and require theory-driven inputs that lie beyond the scope of classical methods. Quantum computation has the potential to enable these calculations, though the underlying hardware requirements remain unclear for many practical applications. We present an end-to-end analysis of how quantum methods could support efforts to isolate cyclic ozone via fullerene encapsulation. Our discussion extends beyond a formal analysis of complexity, providing both logical and physical overhead estimates for ground state energy determinations based on quantum phase estimation (QPE). Taken collectively, these data delineate a plausible scale for realistic, computationally-aided molecular design efforts using fault-tolerant quantum computation.

CONTENTS

I. Introduction	2	1. AzureQRE	10
A. Overview	2	2. pyLIQTR	10
B. Scientific and Commercial Utility	3	B. Resource Estimation Results	10
C. Quantum Computational Approach	4	1. Local Basis: Double-Factorized Hamiltonian	10
II. Workflow and quantum algorithm framework	5	2. Electrostatic Embedding Techniques	11
A. Computational Workflow	5	3. Semilocal Basis: Dual Plane-Wave Hamiltonian	11
B. Qubitized Phase Estimation	6	IV. Conclusion	13
C. Hamiltonian Encodings	8	Acknowledgements	13
1. Local Basis: Double-Factorized Hamiltonian	8	References	14
2. Semilocal Basis: Dual Plane-Wave Hamiltonian	8	A. Complete Workflow for Fullerene-assisted Synthesis of Cyclic Isomer of Ozone	17
III. Resource Estimates	10	1. Formulation and objectives	17
A. Tools and methodology	10	2. Inputs	19
		3. Outputs	19
		4. Workflow Pseudocode	20

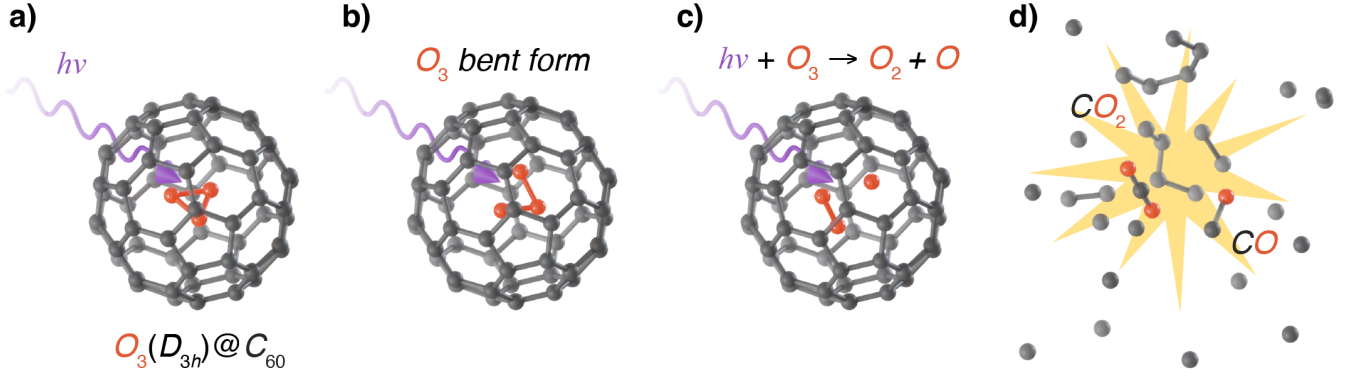


FIG. 1. Proposed photolysis of fullerene-encapsulated cyclic ozone. (a) Cyclic ozone $O_3(D_{3h})$ is isolated in a fullerene matrix, depicted here as C_{60} ; (b) single-photon excitation photoisomerizes $O_3(D_{3h})$ to the conventional bent isomer $O_3(C_{2v})$, inducing molecular strain in already tight geometries; (c) bent ozone undergoes subsequent photolysis into molecular O_2 and atomic oxygen O ; (d) the resulting species react with the fullerene cage through combustion reactions, and foster a sustained burn when numerous oxygen equivalents are present.

I. INTRODUCTION

A. Overview

The development of advanced rocket fuels is critical to the efficiency and performance of future space missions. While fundamentally effective, traditional chemical propellants are often limited in terms of energy density, stability, and environmental impact. These parameters must be balanced when selecting a fuel, and this competition has excluded otherwise appealing candidates. For instance, ozone O_3 has a very favorable energy density, but this is counterbalanced by its excessive reactivity [1]. Ozone's cyclic isomer $O_3(D_{3h})$ [2] is predicted to carry an even higher energy density, though it has not been isolated owing to commensurate instability [3–5].

Recent theoretical efforts suggest that cyclic ozone might be synthesized and stabilized within a fullerene matrix, opening one avenue toward its practical use [6]. This assumption is not with precedent, since geometric confinement is known to shift the relative energetics of different molecular isomers and conformers [1, 6–8]. Moreover, it has been speculated that cyclic H₃ could be stabilized in this manner for hydrogen storage [9]. Cyclic ozone may also have unique features as a propellant, including photochemically initiated combustion. As depicted, ultraviolet light could penetrate a fullerene cage, generating heat and reactive oxygen species through photolysis [10]. Although fullerenes have a nontrivial UV absorption profile — limiting the ultimate optical path depth in a medium — it would still be possible to initiate a vigorously exothermic burn from the boundary. The prospects for controlled energy release, large-scale storage, and safe handling are desirable features in an advanced propellant [7, 8].

While stabilized cyclic ozone is appealing, its synthesis remains a formidable challenge. The leading strategy for fullerene encapsulation leverages a procedure termed *fullerene surgery*. Here, an existing fullerene is opened via cycloaddition reactions or electrocyclic shifts, while leaving a synthetic handle to reseal the cage after introducing a small molecule [11, 12]. The resulting arrangement is termed an endohedral fullerene or endofullerene. This route for encapsulation was proposed in a recent patent for sunscreen, textiles, sunglasses, and wind screens [10]. More specifically, this strategy would sequester oxygen molecules (O_2) in fullerenes of varying size and bombard them with oxygen ions to generate ozone. The stability of any products would be dictated by the size of the fullerene cage and the number of encapsulated oxygen equivalents. By tuning these factors, it may be possible to shift thermodynamic equilibria in favor of ozone's cyclic isomer. Alternatively, optical excitation could be used to generate cyclic ozone *in situ* from its bent counterpart. However, these proposals assume that cyclic ozone would be stable in a fullerene matrix.

The complexity of these experiments would preclude a systematic, trial-and-error strategy. At the minimum, constraints on the target fullerene size and oxygen loading fraction should be known from the outset. An application-oriented perspective would also require some knowledge about reaction mechanism — including photochemical initiation or synthesis — and thus capture prospects for use as a rocket propellant. Accurate reaction energies are particularly relevant when predicting rate constants $k \propto \exp[-\Delta E_a/kT]$, which scale exponentially in ratio of activation energy

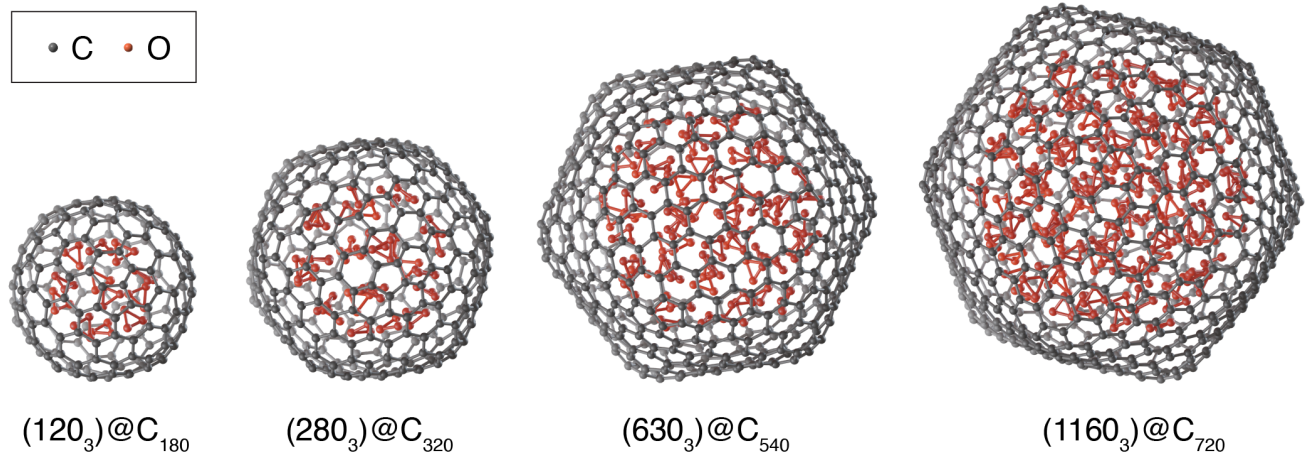


FIG. 2. Relaxed geometries of ozone-containing endofullerenes. Classically optimized geometries of $(x \text{ O}_3(D_{3h}))@\text{C}_n$ for $(x, n) = (12, 180), (28, 320), (63, 540), (116, 720)$, corresponding to utility-scale problem instances that might be solved with quantum computation. Relaxed geometries were obtained using density functional theory (DFT), where electronic structure is described using a PBE+D3 scheme [28, 29] with a GTH pseudopotentials [30] and the TZVP basis set [31]. Calculations were facilitated by the CP2K code [32].

ΔE_a to the thermal energy scale kT . Classical quantum chemical methods formally offer a means to assess the relative energetics of endofullerenes $(x \text{ O}_2, y \text{ O}_3(D_{3h}), z \text{ O}_3(C_{2v}))@\text{C}_n$ and their reactive pathways, where (x, y, z) specify the stoichiometry of oxygen species and n the size of the fullerene (Fig. 2). Unfortunately, ozone's electronic structure and reactivity are characterized by nontrivial non-adiabatic effects and pronounced multireference character [13][14]. This means that most cost-efficient classical computational methods will be inapplicable. While the ground state energy of a single isolated ozone molecule has been computed to high accuracy via the semistochastic heat-bath configuration interaction (SHCI) method, this technique is insurmountably expensive for the minimal example of $\text{O}_3@\text{C}_{60}$ [15].

The electronic structure problem is notoriously difficult due to the exponential scaling between Hilbert space dimension and problem size (e.g., electron filling and orbital count) [16]. This translates to a commensurate overhead in terms of classical resources such as memory and runtime. Quantum computation has the potential to reduce this cost using resources that are polynomial in problem scale. Indeed, quantum chemistry is believed to be one of the first applications that will see a fruitful return from the use of quantum algorithms [17–21]. These prospects have advanced rapidly, resulting in quantum algorithms with reduced resource overhead and the ability to treat more diverse processes such as time-dependent dynamics [22–27].

In this contribution, we estimate the computational cost and practical utility of solving the electronic structure of fullerene-encapsulated cyclic ozone using fault-tolerant quantum computation. We take a holistic approach to utility by including both scientific and economic impacts. Our perspective on quantum computation assumes state-of-the-art algorithms, including qubitized phase estimation (QPE) and efficient block encodings for the electronic structure Hamiltonian. This arrangement would provide energy determinations comparable to FCI in accuracy, yet tackle systems that are intractable through contemporary classical means. We capture this in a concrete setting, adopting the (photo)isomerization reactions $\text{O}_3(D_{3h}) \rightleftharpoons \text{O}_3(C_{2v})$ as a target. A clear perspective on this process would be needed in order to capture thermal stability or the photochemically-aided synthesis or ignition routes. However, the constituent estimates also reflect the scale of other calculations that predict stability. These estimates collectively assess a realistic quantum computational workflow for a practical problem in molecular engineering.

B. Scientific and Commercial Utility

The immediate impact from a synthetic pathway for cyclic ozone is inherently scientific. A leading output from quantum computation would determine if cyclic ozone will be thermodynamically stable in certain fullerene cages. This would establish and justify a procedure to assess general, fullerene-assisted synthesis methods using computational chemistry. Industrial applications lie one step further. Previous synthetic attempts envisioned using shaped laser pulses transform bent ozone into its cyclic structural isomer [3, 4]. The underlying proposition was that cyclic ozone could act as a replacement for liquid oxygen (LOX) or as an additive oxidizing agent in rocket fuel. Realizing

this requires a route to bulk synthesis and capabilities for safe storage. The former would require highly efficient photochemical procedures or confinement–driven formation of the novel oxidant. Value would manifest through the predicted increase in specific impulse, yielding a 33% gain in the amount of payload that each rocket could carry [3].

We consider a case where cyclic ozone or encapsulated cyclic ozone are used as liquid or solid–state propellants, respectively. These could serve as auxiliary fuels or as a standalone replacement for liquid oxygen. The utility of a propellant depends on its specific impulse, the net mass of propellant required for lift, and the complexity of storage and ignition mechanisms. A reusable rocket such as the Falcon heavy can carry 63,800 kg to low–earth orbit (LEO) and 26,700 kg to geostationary transfer orbit (GTO) at a launch cost of \$97M. This equates to \$1,520 per kg to LEO and \$3,633 per kg to GTO [33]. If cyclic ozone allows these rockets to carry one third more payload, this would reflect to an approximate value of \$32M per rocket. SpaceX plans to launch 148 rockets in 2024. If the launch frequency remains constant and all of these are a platform comparable to the Falcon heavy, this would deliver \$47B of value over the next 10 years [34].

This utility argument assumes that (i) cyclic ozone would be stable outside of a fullerene cage and (ii) conversion from cyclic to bent ozone is sufficiently exothermic. When using fullerene–encapsulated ozone, the carbon cage will contribute additional weight while reducing the energy density (though the carbon will also act as an oxidant). It will also modify the propellant containment and ignition mechanisms. This would give a financial utility below free cyclic ozone as a liquid propellant, and thus the aforementioned financial value can be taken as an upper bound. The value of encapsulated cyclic ozone as a solid–state propellant would certainly be large, yet harder to bound since it doesn’t directly substitute for a liquid counterpart. Other use cases include precise thrusters for minor adjustments to satellite trajectories, with an eye towards “micro”– or “nano”–sized satellites with masses between 1.1 to 10 kg [35].

C. Quantum Computational Approach

To understand the feasibility of constructing complex macromolecules — such as endohedral fullerenes — we need to capture the energetics of their reaction pathways. These data are also used to infer stability measures and to assess the viability of rocket propellants. Quantum computing may offer a resource efficient means to handle systems such as ozone, which are characterized by strong multi–reference character and non–adiabatic dynamics. The quantum phase estimation (QPE) algorithm is central to these efforts, and can capture state energies of an electronic structure Hamiltonian with sub–exponential overhead in system size [36]. This is markedly more efficient than comparable classical methods such as the full configuration interaction (FCI), which invariably has exponential overhead and is limited to small systems. The ability to treat large systems the FCI level will translate to increased accuracy (e.g., since QPE could be chosen over approximate classical methods, which are insufficient for this system). There is an important caveat, in that QPE can formally require exponential resources to yield high-precision estimates of ground–state energies with high probability. However, this assumes a poor ansatz for the initial state and tight error thresholds. The problem we consider is highly structured and we do not expect its complexity to scale like the general case.

Our analysis aims to capture the thermal or photo–isomerization between bent and cyclic isomers of an ozone molecule $O_3(C_{2v}) \rightleftharpoons O_3(D_{3h})$ that is sequestered in an endofullerene with other oxygen equivalents. Some isomerization reactions, such as those addressed in our efforts, require a higher level of theory due to subtle energetic differences between participating species or contributions from nuclear quantum effects. Indeed, prior computational studies of this reaction reaction suggest oxygen tunneling may play an important role in the thermal isomerization rate [37].

In the most general case, QPE could be used map a full potential energy surface (PES) for the isomerization reaction. This would involve many calculations with significant quantum resource overhead and overestimates the cost of a utility–scale task. Substantial utility can also be found in augmenting classical calculations, which would require far fewer quantum datapoints. We imagine a kinetic estimation workflow based on variational transition state theory (VTST; Fig. 3), which uses a correction function $\Delta V(s) = V_{HL}(s) - V_{LL}(s)$ to reconcile low–accuracy energies $V_{LL}(s)$ along a reaction coordinate s with counterparts $V_{HL}(s)$ from a higher level of theory. To give a concrete example, the contributions $V_{LL}(s)$ may be taken from density functional theory while $V_{HL}(s)$ would come from a quantum QPE calculation. We may not require $V_{HL}(s)$ for every point along s , as interpolation may be sufficient certain segments. Moreover, some rate–estimation methodologies will only use a subset of these points. VTST and related methods have been quite fruitful for isomerization reactions that involve conical intersections and tunneling phenomena [38, 39].

We adapt an approach that previously captured the thermal stability of an isolated cyclic ozone molecule [37]. Following this method, we require at least four FCI–quality ground state energies $V_{HL}(s)$ along the reaction coordinate. These are taken at the endpoints $s = \pm 1$ where $s = -1$ are reactant (cyclic ozone, $s = -1$) and product (bent ozone, $s = 1$), and at the transition state $s = 0$. We also include an auxiliary point $s_{-1/2} \in [-1, 0]$ that helps determine the correct fitting parameters for the correction function ΔV . This point should not be too close to the transition state.

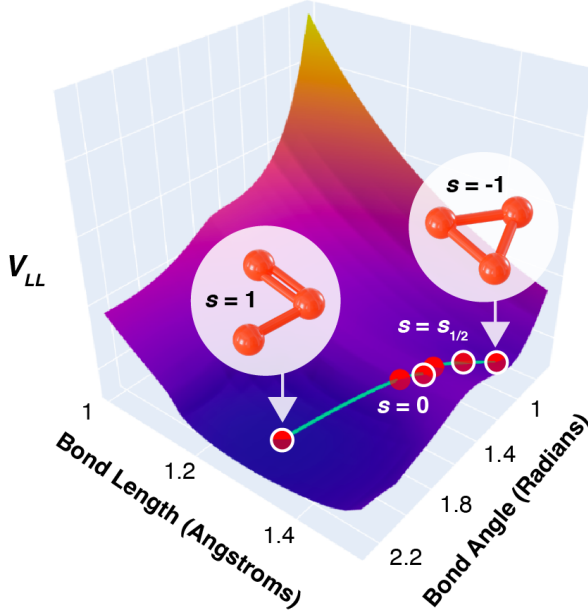


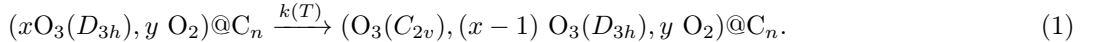
FIG. 3. Potential energy surface for ozone isomerization. The 1^1A_1 ground-state potential energy surface for ozone isomerization is presented at the PBE/GTH/TZVP level, with the minimum energy path (reaction coordinate) between bent ($s = 1$) and cyclic ($s = -1$) isomers depicted as a green line. These data correspond to the low-level contribution V_{LL} from the VTST formalism. The four red points with white circles correspond to the thermodynamic endpoints ($s = \pm 1$) as well as the transition state ($s = 0$) and an additional point used for fitting ($s = 1/2$). The remaining red points capture crossing between the 1^1A_1 ground state and the 1^1A_2 excited state surfaces along the reaction coordinate. Computational methods are identical to those used in Fig. 2.

The thermal isomerization pathway for ozone along a DFT-defined PES is depicted in Fig. 3, and the same conceptual arrangement would be used for photoisomerization on an excited state surface (e.g., following vertical excitation from the ground state surface). We estimate the quantum computational cost of producing FCI-quality energies at points $s = \pm 1, 0, s_{1/2}$ using QPE, assuming that a single ozone isomer is being tracked in the endofullerene ($x \text{ O}_2, y \text{ O}_3$)@C_n. While several structural configurations would likely be sampled in a practical workflow (e.g., such as snapshots from an *ab initio* dynamics trajectory), this gives only a multiplicative factor on top of our estimates.

II. WORKFLOW AND QUANTUM ALGORITHM FRAMEWORK

A. Computational Workflow

Our target is the isomerization rate constant $k(T)$ between cyclic and bent ozone at a fixed temperature T . We assume that this occurs within a fullerene and in the company of other molecular oxygen equivalents:



This reaction underlies the thermal decomposition or photochemical activation of cyclic ozone in a fuel mixture. However, the same computational strategy would apply to reverse reaction, which synthesizes of cyclic ozone from its bent counterpart. Note that structural changes from isomerization can also induce strain the fullerene system, ultimately leading to C–C bond scission and opening of the fullerene cage. This possibility has already been explored in the context of hydrogen storage [9] and could be accommodated in a more comprehensive treatment.

We construct *quantum benchmarking graphs* (QBG) to track the cost of our computation. These are essentially call-graphs at decreasing levels of abstraction, which aggregate the total complexity of all required classical and quantum subroutines (algorithms). The QBG for cyclic ozone is shown in Fig. 4. The highest level of this hierarchy calls a workflow that implements a solution of our application problem. While our analysis is based around VTST, this is

not the only way to handle the underlying tasks. That is, other workflows might populate this level of abstraction with alternative computational methods (e.g. algorithms or sub-workflows implementing these algorithms).

Working within the VTST workflow, the node **Evaluate Stability** applies a series of methods that were introduced in [9, 37] to oxygen-containing fullerenes. This workflow calls **VTST**, which requires quantities such as FCI-quality energies and molecular geometries along the reaction pathway. Our implementation uses quantum phase estimation (QPE) to obtain these energies for a few specific geometries. The geometries, in turn, are derived classically by computing a minimum energy path between reactants and products using the nudged elastic band (NEB) method [40] and density functional theory (DFT) calculations (taken specifically as the **Climbing Image Nudged Elastic Band** (CI-NEB) variant) [41, 42]. Note that NEB accepts atomic forces and energies from DFT, which are passed back as inputs in the QBG.

The remaining classical subroutines generate molecular geometries for various endofullerenes as well as a series of stability parameters [9]. These include the formation energy ΔE and an internal pressure $P(\epsilon)$ exerted by encapsulated molecules on the carbon skeleton. The latter is quantified through the bond strain tensor. Both of these quantities can be obtained using DFT and the geometric arrangement described in 2, where the **TZVP-PBE** node represents and provides low-level energies and atomic forces. These quantities inform us about the stability of the fullerene cage as it confines the ozone molecules. If the temperature rises too high or the cage is filled with too much oxygen, it may rupture and release the encapsulated ozone molecules [9].

Initial geometries are generated by using a sphere packing algorithm to place ozone molecules in a target fullerene. Stated briefly, we can approximate the free volume as a spherical region of radius $R_{\text{free}} = R_0 - R_{\text{vdW}}/2$, where R_0 is the radius of the cage and R_{vdW} is the van der Waals radius of a carbon atom. A similar strategy is used to choose a radius r for spheres that encapsulate the ozone molecules. The resulting geometries are first relaxed using a semiempirical method like the extended tight binding approach (XTB; specifically as the GFN1-xTB method) [43].

The packed geometries are not realistic, finite-temperature atomic configurations. To remedy this, the QBG workflow samples coordinates from *ab initio* molecular dynamics (MD) simulations that are based on tight-binding DFT (XTB) and a Langevin thermostat. We utilize a method based on [44, 45] as implemented in CP2K [32]. While Langevin dynamics can have unphysical kinetics, they rapidly sample a physically meaningful ensemble. The inputs for our resource estimates were prepared using this scheme. Note that we couple only the fullerene atoms to the Langevin bath and integrate equations of motion using a classical Trotter–Suzuki integrator (coupling frequency $\gamma = 0.005 \text{ fs}^{-1}$; timestep of $\delta = 0.5 \text{ fs}$) [44]. This gives a natural arrangement where the cage links to the broader environment, with minimal kinetic artifacts for the oxygen atoms [46]. This is followed by full DFT relaxation using the PBE density functional and a D3 dispersion correction, alongside the TZVP basis [31] and GTH pseudopotentials [30]. A comparable scheme was previously shown to give reasonable geometries for chemically similar systems [6, 47, 48].

The last component is a classical algorithm that prepares the initial state for quantum phase estimation. The **DMRG** and **Selected CI** methods both accomplish this task and there are efficient methods to load these outputs into quantum computers [49, 50]. However, the overlap between the initial guess and the true ground state will influence the number of QPE circuit shots (Fig. 5) that are needed to obtain chemical accuracy in our energy estimates (defined as 1.6 mHa). This critical detail puts fixed-basis electronic structure into the QMA-complete complexity class, which is the quantum analogue of NP-complete. It is provably hard for quantum computers to solve these problems and that fact can compromise an exponential speedup [51]. We can always select for classically intractable chemistry problems that are in a “goldilocks zone” with sufficient overlap between our guess and the true ground state (e.g., impurity Hamiltonians beyond the free fermion picture and their hidden variants) [52–54]. A sufficient overlap is likely for the computational tasks that we describe. However, these considerations ultimately mean that QPE is heuristic and capturing its true performance will require a comparison of different approaches to generating the initial guess.

B. Qubitized Phase Estimation

Many ground-state estimation protocols are based on the quantum phase estimation (QPE) algorithm [55]. A qubitized variant of this method can markedly improve runtime efficiency by encoding electronic spectra of the Hamiltonian H in a Szegedy walk operator W [56–58]. Loosely stated, qubitization describes a strategy that encodes a normalized, non-unitary operator H/λ within a designated block of a larger unitary operator U_H [22]. The factor λ is normalization that ensures unitarity. This gives an effective two-dimensional Hilbert space for each eigenvalue E_k , which is spanned by the eigenstate and its orthogonal complement. The resulting walk operator assumes a particularly useful form on each space,

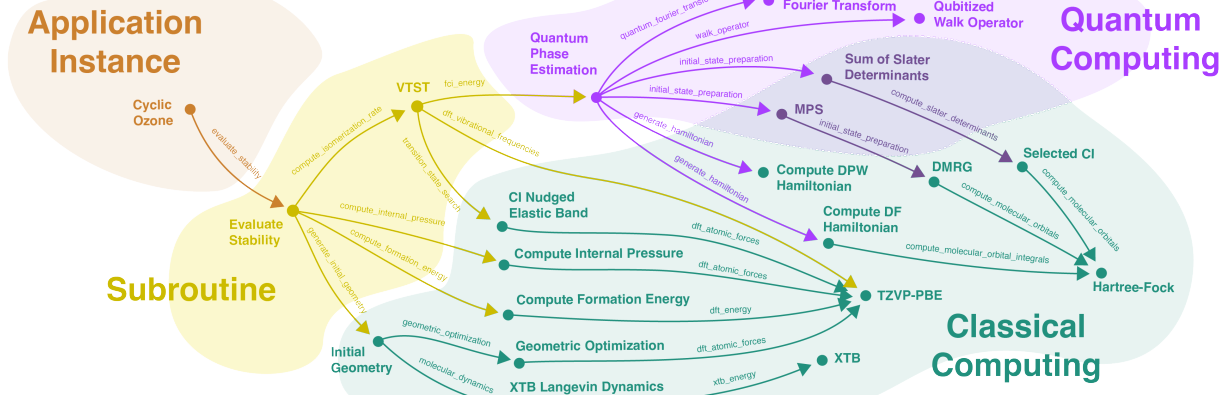


FIG. 4. A Quantum Benchmarking Graph (QBG) for ozone isomerization. This callgraph captures a full computational workflow, including both quantum and classical subroutines. Arrows point to nodes that provide a required action/quantity, as specified by the edge labels between nodes. Each colored region represents a different level of abstraction, while classical and quantum components are divided into separate green and purple regions, respectively. Note that the arrows also show how the classical and quantum subroutines exchange data such as molecular geometries, ground state energies, Hamiltonians, and initial classical guesses for the ground state.

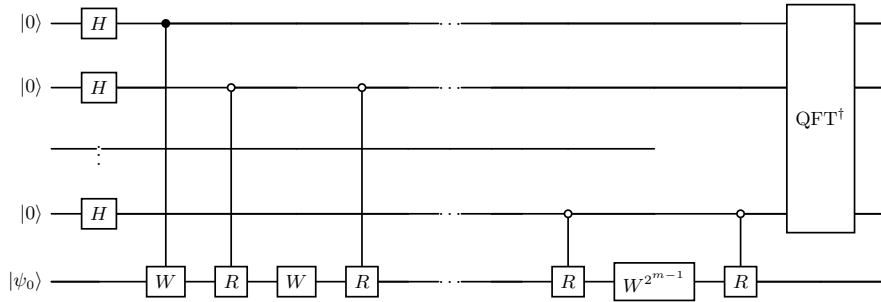


FIG. 5. Quantum circuit implementing qubitized phase estimation. This implementation queries powers of the qubitized walk operator W instead of the standard time evolution oracle. The eigenphases ϕ_k of W have a simple functional relation with the eigenenergies E_k of a target Hamiltonian H . Specifically, $\phi_k = \arccos(E_k/\lambda)$, where λ is a normalization factor for the block encoding of H . This relationship allows us to extract the eigenenergies using phase estimation.

$$W = \begin{pmatrix} \frac{E_k}{\lambda} & \sqrt{1 - \left(\frac{E_k}{\lambda}\right)^2} \\ -\sqrt{1 - \left(\frac{E_k}{\lambda}\right)^2} & \frac{E_k}{\lambda} \end{pmatrix} = e^{i \arccos(E_k/\lambda) Y} \quad (2)$$

where Y denotes the corresponding Pauli operator. Notably, this gives a simple functional relationship $\phi_k = \arccos(E_k/\lambda)$ between eigenphases and eigenenergies for a given Hamiltonian. By extending this convention to QPE, an eigenenergy can be estimated to a precision of ΔE by using $m = [\log_2(\sqrt{2\pi}\lambda/2\Delta E)]$ precision qubits (ancilla). A circuit implementing this QPE approach is depicted in Fig. 5 and a circuit for the qubitized walk W is given in Fig. 6

Here, the data register is prepared in a state that overlaps significantly with the ground state. The success probability in postselection depends on this overlap, so it is important that it is high (see [36] for an analysis of the resulting complexity). The walk operator is assembled using PREPARE and SELECT oracles, which is a standard strategy to block encode Hamiltonians following the Linear Combination of Unitaries (LCU) access model [22, 59, 60]. At the end of the circuit, an inverse quantum Fourier transform (QFT) allows the accumulated phase to read off the ancilla in a bitwise manner. We defer to the discussion in [58] for further details.

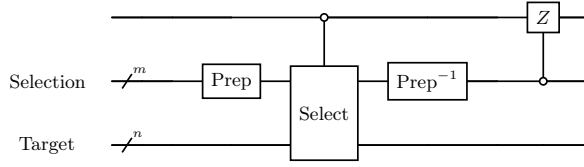


FIG. 6. Qubitized Walk Operator. The walk operator W is implemented via Prepare and Select oracles, which specify a block encoding for the Hamiltonian H , and a multicontrolled CZ gate which gives a reflection in each qubitized subspace. The selection qubits are a set of $m = \lceil \log_2 n \rceil$ ancilla that implement the block encoding and the target is an n -qubit state.

C. Hamiltonian Encodings

Endofullerenes such as $(12\text{ O}_3)\text{@C}_{180}$ are larger than the molecules typically studied using post–Hartree–Fock techniques. These molecules also lack the clear periodic structure of condensed matter systems. These factors present a challenge for algorithm selection. We describe and estimate resources using multiple methods, allowing us to capture the landscape of possible Hamiltonian encodings and the resulting effect overhead. All of these methods could provide sufficient accuracy if the underlying scale parameters (e.g., size of the active space, number of dual plane waves) are large enough to capture electronic wavefunction.

1. Local Basis: Double–Factorized Hamiltonian

Small–molecule quantum chemistry is typically handled using a local orbital basis. While a full set of these classical orbitals could be included in our quantum calculation, this generally gives excessive overhead and a diminishing return. We will instead use an *active space* approach, which conjoins an effective Hamiltonian with a smaller set of problem–adapted orbitals (often tens to hundreds for small molecules). We define an initial, classical electronic structure using Hartree–Fock with a minimal STO–3G [61] basis set for fullerene carbons and a larger cc–pVDZ [62] basis for the oxygen atoms. The result describes $(12\text{ O}_3)\text{@C}_{180}$ using a total of 1404 orbitals. This output is then used to define active spaces of increasing size via the AVAS method [63], as facilitated by the PySCF [64] code. Our procedure delivers coefficients for the standard quantum chemistry Hamiltonian,

$$H = \sum_{ij,\sigma} h_{ij} a_{i\sigma}^\dagger a_{i\sigma} + \frac{1}{2} \sum_{ijkl,\sigma\rho} h_{ijkl} a_{i\sigma}^\dagger a_{k\rho}^\dagger a_{l\rho} a_{j\sigma}, \quad (3)$$

where h_{ij} and h_{ijkl} are the one– and two–electron integrals, σ and ρ index spin, and $a_{p\sigma}$ are fermionic creation and annihilation operators. There is considerable overhead when encoding this Hamiltonian for use on a quantum computer. Instead, we opt to use a more resource–efficient encoding known as double–factorization [65].

To understand this, note that the fourth–order Coulomb tensor h_{ijkl} can be rearranged into a $N^2 \times N^2$ matrix, where N is the number of *spin orbitals*. This is termed the electronic repulsion integral (ERI) matrix A , which is positive semi-definite and exhibits a rank $L = O(N)$ for chemical systems. Diagonalizing A gives a set of eigenvalues λ_ℓ and eigenvectors v_ℓ that are of dimension N^2 . The double factorized Hamiltonian H_{DF} is then constructed from H and the set $\{(v_\ell, \lambda_\ell)\}_{\ell=0}^{L-1}$ as:

$$H_{\text{DF}} = \sum_{ij,\sigma} h_{ij} a_{i\sigma}^\dagger a_{j\sigma} + \frac{1}{2} \sum_{\ell=0}^{L-1} \lambda_\ell \left(\sum_{ij,\sigma} [v_\ell]_{ij\sigma} a_{i\sigma}^\dagger a_{j\sigma} \right)^2. \quad (4)$$

This double factorized Hamiltonian H_{DF} can be efficiently translated into the walk operator W that is required for QPE, as described in Ref. [65].

2. Semilocal Basis: Dual Plane–Wave Hamiltonian

The dual plane–wave (DPW) basis is constructed as the Fourier transform of a nonlocal plane–wave (PW) basis, and corresponds to semilocal functions that are arranged on a regular real–space grid. This scheme has certain

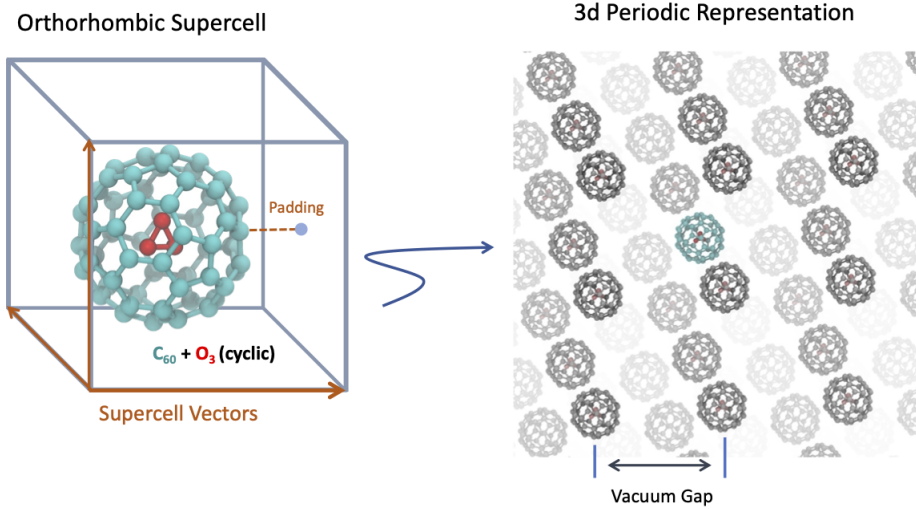


FIG. 7. Endofullerene in a periodic supercell. Geometry of an ozone-containing endofullerene $O_3@C_{60}$ embedded in an orthorhombic supercell. Note the vacuum padding that flanks the fullerene cage. This ultimately defines the geometric separation between periodic images.

advantages for quantum algorithms — such as a favorable $O(N^2)$ scaling for terms in the Coulomb tensor — though it assumes a periodic system. We can nonetheless treat isolated molecules like our endofullerenes by separating periodic images with a vacuum gap. This gap should be large enough to attenuate electrostatic self-interaction and to prevent wavefunction ‘leakage’ across periodic boundaries (Fig. 7). The N -spin-orbital (basis element) DPW electronic structure Hamiltonian takes the form:

$$\begin{aligned} H &= \sum_{pq,\sigma} T(p-q) a_{p\sigma}^\dagger a_{q\sigma} + \sum_{p\sigma} U(p) n_{p\sigma} + \sum_{(p\alpha) \neq (q\beta)} V(p-q) n_{p\alpha} n_{q\beta} \\ &= \underbrace{\frac{1}{N} \sum_{pq,\sigma,\nu} k_\nu^2 \cos [k_\nu \cdot r_{p-q}] a_{p\sigma}^\dagger a_{q\sigma}}_{\text{kinetic}} - \underbrace{\frac{4\pi}{\Omega} \sum_{p\sigma,j\nu \neq 0} \frac{\zeta_j \cos [k_\nu \cdot (R_j - r_p)]}{k_\nu^2} n_{p\sigma}}_{\text{electron-ion}} + \underbrace{\frac{2\pi}{\Omega} \sum_{(p\alpha) \neq (q\beta)} \frac{\cos [k_\nu \cdot r_{p-q}]}{k_\nu^2} n_{p\alpha} n_{q\beta}}_{\text{electron-electron}} \end{aligned}$$

where the fermionic operators $a_{p\sigma}^\dagger$ and $a_{p\sigma}$ now act on a spatial spin orbital p and where $n_{p\sigma} = a_{p\sigma}^\dagger a_{p\sigma}$ is the number operator. Each orbital is associated with an orbital centroid,

$$r_p = p \left(\frac{2\Omega}{N} \right)^{1/3},$$

where Ω is the computational cell volume and R_j is the position of atom j with atomic number ζ_j . The momentum modes are defined as,

$$k_\nu = 2\pi \frac{\nu}{\Omega^{1/3}},$$

with $\nu \in [-(N/2)^{1/3}, (N/2)^{1/3}]^3$. This closely follows the notion of [58]. As noted earlier, the number of electron-electron interaction terms scales as $O(N^2)$, while they scale as $O(N^3)$ in a plane-wave basis and $O(N^4)$ using Gaussian type orbitals. While kinetic terms also scale as $O(N^2)$ in the DPW basis (as opposed to $O(N)$ as in the plane-wave basis) this increase is offset by reduced complexity of the Coulomb tensor. A key parameter for this method is the distance a_0 between adjacent points in the real-space basis grid. In principle, this lengthscale can be loosely related $a_0 \approx \sqrt{2\pi^2/E_{\text{cut}}}$ to the energy cutoff E_{cut} for some equivalent plane-wave calculation (i.e., formally via a Fourier transform). However, there will be some degree of ambiguity when translating convergence with momentum-space pseudopotentials to their real-space counterparts.

III. RESOURCE ESTIMATES

Asymptotic scaling can give a misleading impression of computational overhead, since many problems are of a size where algorithmic prefactors and subleading contributions can be relevant. This becomes especially pronounced when we consider specific Hamiltonian encodings. We avoid this complication by explicitly counting resources using a detailed profiling strategy and explicit circuit constructions. These tasks are facilitated by the Azure Quantum Resource Estimator [66, 67] and the pyLIQTR toolkit [68], respectively.

A. Tools and methodology

1. AzureQRE

The Azure Quantum Resource Estimator (AzureQRE) [66, 67] is a component of the Azure Quantum Development Kit [69], which handles both logical and hardware-level estimation. At the application level, we set an accuracy threshold of 1 mHa for energy determinations. This is below the standard chemical accuracy of 1.6 mHa. The hardware level estimates use the `qubit_gate_ns_e4` model within AzureQRE, which assumes an optimistic superconducting device (e.g., transmon qubits) having 50 ns gate times, 100 ns measurement times, and error rates of 10^{-4} for both Clifford and non-Clifford mechanisms. We set a total error budget of 1%. Logical circuits implementing the double-factorized qubitization algorithm [65] are compiled within Q# and passed into the physical resource estimator. Fault-tolerance is handled through a surface code [70] implementation on a 2D nearest-neighbor layout that is capable of parallel operations. The overhead of logical qubit movement and multi-qubit measurements using lattice surgery operations is included [71, 72]. T -gates are implemented through a magic state distillation protocol in dedicated factories [73]. More detail regarding the architectural assumptions used in AzureQRE are described elsewhere [67].

2. pyLIQTR

The pyLIQTR toolkit implements a range of quantum algorithms that can be analyzed at the logical level. A distinguishing characteristic of pyLIQTR is its hierarchical nature, where the top-level circuit is an entire qubitized algorithm. This is decomposed in stages, yielding progressive subcircuits that are ultimately translated into the Clifford+ T gate set. Such modularity leads to efficient resource estimation, since repeated elements can be analyzed once and cached for later use. We use pyLIQTR for our DPW resource estimates.

The DPW grid spacing was chosen to match energy cutoffs from a previously benchmarked PW pseudopotential scheme. Ultrasoft pseudopotential calculations suggest that an $E_{\text{cut}} = 40$ Ry cutoff would be sufficient for this system, which corresponds to a separation of $a_0 = 0.526$ Å between the loci for DPW basis functions. We assume that an equivalent DPW pseudopotential can be absorbed into the Hamiltonian coefficients, but do not attempt to make this quantitative (this should only impact the encoding normalization). Molecules were isolated from their periodic images using a 10 Å vacuum padding and explicit Hamiltonian coefficients were generated from target molecular geometries using pyLIQTR's PEST module. These data were passed to the pyLIQTR circuit generation framework, which implements a block encoding for DPW electronic structure with linear T -complexity in problem size [58]. The result defines a walk operator for qubitized phase estimation. Explicit circuits were generated assuming a target accuracy of 1 mHa for energy estimations. This formed the foundation for our resource estimates.

For a given circuit, the resources reported by pyLIQTR include logical qubits, T -gates, and Clifford gates. This includes contributions from rotation synthesis, which are estimated using a heuristic model that depends on the user specified rotation gate precision. Our targeted energy error of 10^{-3} implies an upper bound on this precision should be on the order of 10^{-6} . We ultimately adopt a precision of 10^{-10} , which ensures that rotation synthesis will be a limiting factor. However, this also implies that our resource estimate values will constitute an upper bound.

B. Resource Estimation Results

1. Local Basis: Double-Factorized Hamiltonian

The logical and physical resource overhead for a single-shot QPE calculation are depicted in Fig. 8. These data assume active spaces of varying size for the $(12 \text{ O}_3)@\text{C}_{180}$ system and a double-factorized Hamiltonian encoding. The underlying numerical values and surface code parameters are provided in Table I. At the logical level, we see that

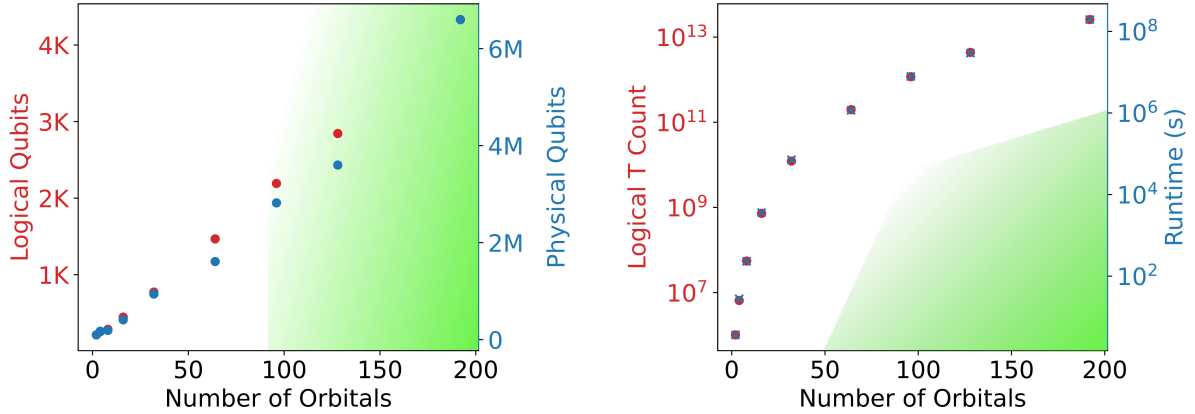


FIG. 8. **Resource estimates for QPE with double-factorized Hamiltonians.** Logical and physical resource estimates are provided for the $(12 \text{ O}_3)@\text{C}_{180}$ system. These data are parameterized by the number of orbitals N_{orb} in increasingly large active spaces (in terms of spin orbitals, $N = 2N_{\text{orb}}$). Estimates correspond to (a) the number of logical and physical qubits and (b) the logical T -count and total runtime. Physical estimates assume a fault tolerant layer based on the surface code and an idealized superconducting architecture. Further details regarding these estimates are presented in Table I. The shaded green region represents an approximate notion of where quantum computation may have utility for this problem. Points in the green region could be populated improvements in hardware, problem encoding, and circuit compilation.

this algorithm has a spatial overhead of roughly 20 logical qubits per orbital. The temporal resource requirements are also substantial, with the smallest active space — which is classically trivial — requiring approximately 10^6 T -gates. Conversely, the largest, maximal-performance active space requires over 4000 logical qubits and 2.6×10^{13} T -gates. This leads to hefty physical overhead from the error-correction layer, and we estimate that approximately 6×10^6 physical qubits for a $d = 19$ surface code implementation (the code distance is fixed to satisfy our error budget for a given active space). Assuming the idealized superconducting architecture detailed earlier, we estimate the runtime for this largest instance to be slightly over six years. However, it is unlikely that an active space this large would be needed for meaningful insights.

2. Electrostatic Embedding Techniques

Our energy estimates correspond to a fixed atomic geometry. Moreover, the carbon-based skeleton should only make a weak contribution to the electronic structure of ozone — instead, it likely tunes ozone’s orbital architecture through electrostatic perturbations. This suggests that we could omit the fullerene from our active space and treat it as a point charge distribution. The logical overhead for this electrostatic embedding scheme is captured for a simple $(\text{O}_3)@\text{C}_{60}$ endofullerene in Fig. 9. The overhead for this scheme was estimated to a CAS(22, 14) active space by using pyLIQTR to generate explicit QPE circuits for a double-factorized encoding. While these are all classically tractable instances, it is instructive to compare the results with the local-basis estimates from Fig. 8. These two estimates use different tool chains and address molecules of different size. However, the leading overhead is largely tied to the active space size (while other features enter through the encoding normalization). In the case of a 16 orbital active space, we find that the preceding calculations require 7.26×10^8 T -gates, while the embedding scheme requires 1.23×10^8 T -gates. While this reduction is minor, it still constitutes a decrease in resource overhead. This strategy could be fruitful for larger endofullerenes such as $(12\text{O}_3)@\text{C}_{180}$, where the underlying O_3 orbitals will be largely isolated from the fullerene skeleton.

3. Semilocal Basis: Dual Plane-Wave Hamiltonian

The overhead for QPE with a nonlocal DPW basis is presented in Fig. 10. These estimates are derived using explicit circuits from pyLIQTR, including a block encoding with linear T -complexity in orbital count. Here, the number of basis functions is determined by the DPW grid spacing, which we map to an equivalent plane-wave cutoff. The overhead for these calculations would be substantially larger than those based on the local basis scheme. The increased cost is associated with the number of basis functions required for the real-space grid, which includes a large

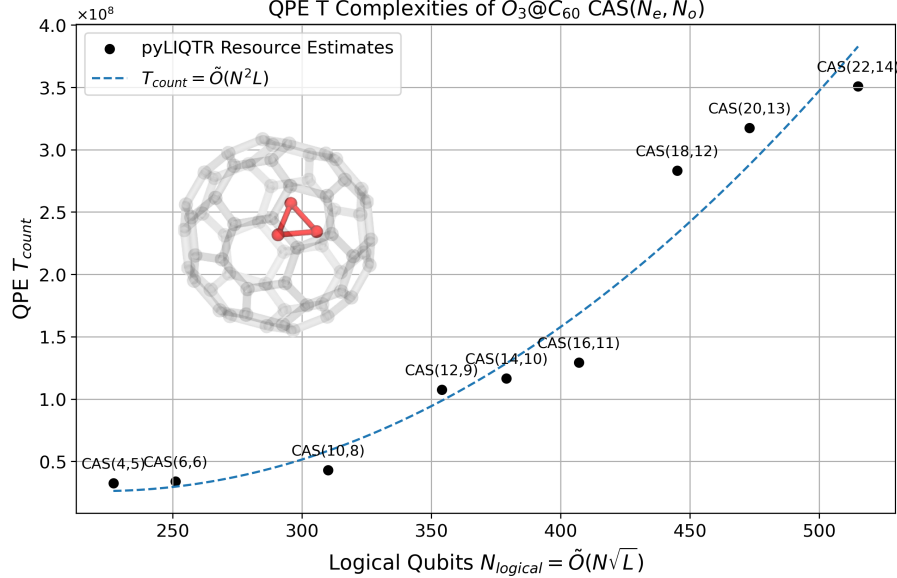


FIG. 9. **Electrostatic embeddings for double-factorized electronic structure.** The resource overhead for the $O_3@C_{60}$ system quantified for a case where the fullerene cage is treated as a simple point charge distribution (via the frozen core approximation). The fit $N_T = \tilde{O}(N_{\text{orb}}^2 L) = \tilde{O}(N_{\text{logical}}^2)$ tracks the relationship between T -gate count N_T and logical qubit count N_{logical} , as parameterized by the number of active space orbitals N_{orb} and the rank L of the factorized Coulomb tensor h_{ijkl} (where $N = 2N_{\text{orb}}$ in terms of spin orbitals). Classical inputs are based of Hartree–Fock with a cc-pVTZ basis. These classical calculations were performed using NWChem [74] and resource estimation is based on explicit circuits from pyLIQTR.

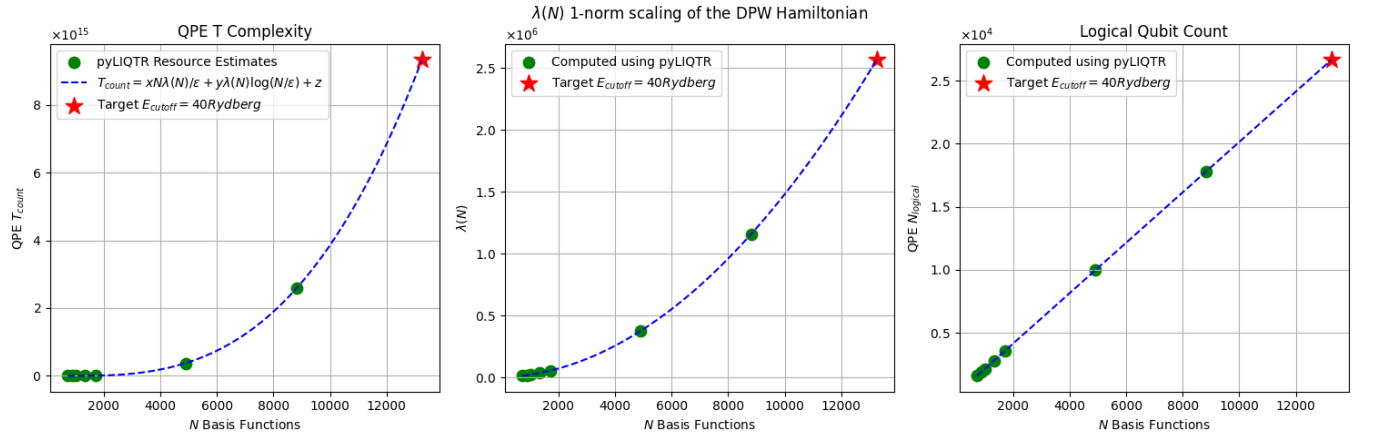


FIG. 10. **Resource estimates for QPE in a dual plane-wave basis.** Estimates are provided for the $O_3(D3h)@C_{60}$ system, using an encoding with a linear T -complexity in the number of basis functions. Data capture scaling of (a) temporal overhead via the T -count; (b) the normalization factor λ for the block encoding; and (c) the number of logical qubits that are required for a single-shot calculation.

number of points in the vacuum layer. This is invariably less efficient than the effective models based on active spaces from the preceding sections. We estimate nearly 1×10^{16} T -gates would be required for this largest system, with a spatial overhead of approximately 2.5×10^4 logical qubits.

N_{orb}	Logical QB	T -count	Distance	Physical QB	T -factories	Physical QB / Factory	Runtime (s)
2	214	1.02e6	9	9.79e4	11	2.16e4	3.63
4	255	6.55e6	11	1.74e5	12	3.89e4	27.73
8	287	5.51e7	11	1.90e5	12	3.89e4	230.88
16	446	7.26e8	13	4.09e5	15	8.64e4	3.62e3
32	773	1.23e10	15	9.40e5	13	2.08e5	7.13e4
64	1.47e3	1.98e11	15	1.61e6	15	2.40e5	1.16e6
96	2.19e3	1.17e12	17	2.82e6	13	2.08e5	7.87e6
128	2.84e3	4.37e12	17	3.60e6	14	2.24e5	2.95e7
192	4.33e3	2.58e13	19	6.60e6	13	2.08e5	1.95e8

TABLE I. Parameters underlying QPE estimates for double-factorized Hamiltonians. Exact estimates and parameters for the fault-tolerant layer correspond to the data of Fig. 8. Data correspond to QPE for the $(12 \text{ O}_3)@\text{C}_{180}$ system for active spaces containing $N = 2N_{\text{orb}}$ spin orbitals.

IV. CONCLUSION

This contribution captures an industrially-relevant application for quantum computation, namely assessing the stability of cyclic ozone in an endofullerene matrix. This is flanked by a classical workflow that addresses geometry of oxygen-containing endofullerenes and prepares inputs for its quantum counterpart. While our estimates have only explicitly addressed the cost of calculations for isomerization, the single-point energy evaluations used to describe photoisomerization on an excited state surface would have comparable overhead.

The utility of this workflow would be maximized as a high-accuracy “black-box” for electronic structure predictions. This could support the direct, quantitative design of new fuel mixtures through a pseudo-combinatorial search over fullerene geometries and atomic configurations. However, this would also require a large number of calculations with nontrivial resource overhead. We argue that a less ambitious approach would have comparable utility. Here, a curated set of calculations would explore thermal stability or photoactivation and derive heuristics that guide experiment. The same principle would extend to other reactions, such as those underlying fullerene surgery [12] and the reaction of oxygen equivalents with the fullerene environment. This follows the general spirit of our workflow, where techniques like VTST are used to simplify rate predictions and leverage classical methods where they have sufficient accuracy. That is, we are able to maximize efficiency by limiting quantum computation to cases where it would be truly impactful.

Endofullerenes present an interesting problem scale for quantum computation. These are spatially isolated systems with computational tasks that involve the reactivity of small molecules. However, the number of atoms is much larger than many quantum-relevant problems in small-molecule chemistry, such as catalysis. We captured the overhead for these systems using several algorithmic techniques — including encodings for local and semilocal bases — as well as an electrostatic embedding strategy. Our classical estimates are in line with other efforts, which have found that significant quantum resources will be required to capture reactivity [75–77]. That being said, there remains a reason for optimism. A calculation with entry-level utility (e.g., a 64-orbital active space) may require roughly $10^{11} T$ -gates per shot with a predicted runtime of 13.43 days. This lies just beyond the scale commonly accessed using classical tensor-network methods (these are generally approximate). While the largest active space (192 orbitals) would require on the order of $10^{13} T$ -gates and a runtime of roughly three years, it is not unreasonable that algorithmic improvements could ultimately reduce this by two orders of magnitude. Recent developments based on tensor hypercontraction [24, 78] and compressed double-factorization [79] have yielded more efficient Hamiltonian encodings, and alternative methods invoking first-quantized electronic structure [78] can lower logical overhead. To put this in context, tensor hypercontraction only required ~ 1500 logical qubits and 7×10^9 Toffoli gates [77] to describe reactivity at the catalytic center of cytochrome p450 enzymes. Given the assumptions underlying our analysis, the associated single-shot runtime would be comparable to relatively trivial calculations in classical quantum chemistry.

ACKNOWLEDGEMENTS

All authors except JEE, KJM, and KMO acknowledge support by the Defense Advanced Research Projects Agency under Contract No. HR001122C0074. JEE, KJM, and KMO separately acknowledge support from the Defense Advanced Research Projects Agency under Air Force Contract No. FA8702-15-D-0001. Any opinions, findings and conclusions or recommendations expressed in this material are those of the authors and do not necessarily reflect

the views of the Defense Advanced Research Projects Agency. MJB acknowledges the support of the ARC Centre of Excellence for Quantum Computation and Communication Technology (CQC2T), project number CE17010001.

The authors thank John Carpenter for his support in creating high-resolution figures for this paper. We would like to thank Marc Dvorak, Steven Cotton, Elias Lawson–Fox and Coleman Scott for helpful discussions.

- [1] J.-L. Chen and W.-P. Hu, Theoretical prediction on the thermal stability of cyclic ozone and strong oxygen tunneling, *Journal of the American Chemical Society* **133**, 16045 (2011).
- [2] We will differentiate bent O₃(C_{2v}) and cyclic O₃(D_{3h}) isomers of ozone by appending the Schoenflies symbol for the latter. The symmetry group will be omitted for the bent form by convention.
- [3] Temple Researcher Attempting To Create Cyclic Ozone.
- [4] R. J. Levis, D. A. Romanov, H. A. Rabitz, Y. G. Kevrekidis, and R. Coifman, *Photonic Reagents: The Production of Cyclic Ozone, With a Focus on Developing Equation Free Methods for Optimization Schemes*, Tech. Rep. (TEMPLE UNIV PHILADELPHIA PA, 2008).
- [5] R. Plass, K. Egan, C. Collazo-Davila, D. Grozea, E. Landree, L. D. Marks, and M. Gajdardziska-Josifovska, Cyclic ozone identified in magnesium oxide (111) surface reconstructions, *Physical Review Letters* **81**, 4891 (1998).
- [6] D. S. Sabirov and I. S. Shepelevich, Information entropy of oxygen allotropes. a still open discussion about the closed form of ozone, *Computational and Theoretical Chemistry* **1073**, 61 (2015).
- [7] H. W. Kroto, J. R. Heath, S. C. O'Brien, R. F. Curl, and R. E. Smalley, C60: Buckminsterfullerene, *Nature* **318**, 162 (1985).
- [8] M. Saunders, H. A. Jiménez-Vázquez, R. J. Cross, and R. J. Poreda, Stable compounds of helium and neon: He@C 60 and ne@C 60, *Science* **259**, 1428 (1993).
- [9] O. V. Pupysheva, A. A. Farajian, and B. I. Yakobson, Fullerene nanocage capacity for hydrogen storage, *Nano Letters* **8**, 767 (2007).
- [10] S. Naseri and M. Bock, Endohedral fullerenes having enclosed therein one or more ozone molecules, and their use as a uv-absorbing agent (2014), uS Patent 8,623,337.
- [11] M. Murata, Y. Murata, and K. Komatsu, Surgery of fullerenes, *Chemical Communications* , 6083 (2008).
- [12] S. Bloodworth and R. J. Whitby, Synthesis of endohedral fullerenes by molecular surgery, *Communications Chemistry* **5**, 121 (2022).
- [13] D. Theis, J. Ivanic, T. L. Windus, and K. Ruedenberg, The transition from the open minimum to the ring minimum on the ground state and on the lowest excited state of like symmetry in ozone: A configuration interaction study, *The Journal of Chemical Physics* **144**, 104304 (2016).
- [14] The term multireference is used in the chemistry community to describe an electronic structure that isn't captured by a single Slater determinant (e.g., as might be obtained from a Hartree–Fock calculation) [80–82]. Instead, they require a linear combination of multiple reference states in order to fully resolve the strong correlation present in the electronic structure.
- [15] A. D. Chien, A. A. Holmes, M. Otten, C. J. Umrigar, S. Sharma, and P. M. Zimmerman, Excited states of methylene, polyenes, and ozone from heat-bath configuration interaction, *The Journal of Physical Chemistry A* **122**, 2714 (2018).
- [16] S. McArdle, S. Endo, A. Aspuru-Guzik, S. C. Benjamin, and X. Yuan, Quantum computational chemistry, *Reviews of Modern Physics* **92**, 015003 (2020).
- [17] G. Ortiz, J. E. Gubernatis, E. Knill, and R. Laflamme, Quantum algorithms for fermionic simulations, *Physical Review A* **64**, 022319 (2000).
- [18] I. Kassal, S. P. Jordan, P. J. Love, M. Mohseni, and A. Aspuru-Guzik, Polynomial-time quantum algorithm for the simulation of chemical dynamics, *Proceedings of the National Academy of Sciences* **105**, 18681 (2008).
- [19] B. P. Lanyon, J. D. Whitfield, G. Gillett, M. E. Goggin, M. P. Almeida, I. Kassal, J. D. Biamonte, M. Mohseni, B. J. Powell, M. Barbieri, A. Aspuru-Guzik, and A. G. White, Towards quantum chemistry on a quantum computer, *Nature chemistry* **2**, 106 (2009).
- [20] M. Reiher, N. Wiebe, K. M. Svore, D. Wecker, and M. Troyer, Elucidating reaction mechanisms on quantum computers, *Proceedings of the National Academy of Sciences* **114**, 7555 (2017), <https://www.pnas.org/content/114/29/7555.full.pdf>.
- [21] B. Bauer, S. Bravyi, M. Motta, and G. K.-L. Chan, Quantum algorithms for quantum chemistry and quantum materials science, *Chemical Reviews* **120**, 12685 (2020).
- [22] G. H. Low and I. L. Chuang, Hamiltonian Simulation by Qubitization, *Quantum* **3**, 163 (2019).
- [23] G. H. Low and N. Wiebe, Hamiltonian simulation in the interaction picture (2018), [arXiv:1805.00675](https://arxiv.org/abs/1805.00675).
- [24] J. Lee, D. W. Berry, C. Gidney, W. J. Huggins, J. R. McClean, N. Wiebe, and R. Babbush, Even more efficient quantum computations of chemistry through tensor hypercontraction, *PRX Quantum* **2**, 030305 (2021).
- [25] R. Babbush, N. Wiebe, J. McClean, J. McClain, H. Neven, and G. K.-L. Chan, Low-depth quantum simulation of materials, *Physical Review X* **8**, 011044 (2018).
- [26] R. Babbush, C. Gidney, D. W. Berry, N. Wiebe, J. McClean, A. Paler, A. Fowler, and H. Neven, Encoding electronic spectra in quantum circuits with linear t complexity, *Physical Review X* **8**, 10.1103/physrevx.8.041015 (2018).
- [27] D. W. Berry, D. Motlagh, G. Pantaleoni, and N. Wiebe, Doubling efficiency of hamiltonian simulation via generalized quantum signal processing (2024), [arXiv:2401.10321](https://arxiv.org/abs/2401.10321).

- [28] P. Perdew, K. Burke, and M. Ernzerhof, Generalized Gradient Approximation Made Simple, *Physical Review Letters* **77**, 3865 (1996).
- [29] S. Grimme, J. Antony, S. Ehrlich, and H. Kreig, A consistent and accurate ab initio parametrization of density functional dispersion correction (DFT-D) for the 94 elements H-Pu , *The Journal of Chemical Physics* **132**, 154104 (2010).
- [30] S. Goedecker, M. Teter, and J. Hutter, Separable dual-space Gaussian pseudopotentials, *Physical Review E* **54**, 1703 (1996).
- [31] A. Schaefer, C. Huber, and R. Ahlrichs, Fully optimized contracted Gaussian–basis sets of triple zeta valence quality for atoms Li to Kr, *The Journal of Chemical Physics* **100**, 5829 (1994).
- [32] T. D. Kühne, M. Iannuzzi, M. Del Ben, V. V. Rybkin, P. Seewald, F. Stein, T. Laino, R. Z. Khaliullin, O. Schütt, F. Schiffmann, D. Golze, J. Wilhelm, S. Chulkov, M. H. Bani-Hashemian, V. Weber, U. Boršnik, M. Taillefumier, A. S. Jakobovits, A. Lazzaro, H. Pabst, T. Müller, R. Schade, M. Guidon, S. Andermatt, N. Holmberg, G. K. Schenter, A. Hehn, A. Bussy, F. Belleflamme, G. Tabacchi, A. Glöck, M. Lass, I. Bethune, C. J. Mundy, C. Plessl, M. Watkins, J. VandeVondele, M. Krack, and J. Hutter, Cp2k: An electronic structure and molecular dynamics software package - quickstep: Efficient and accurate electronic structure calculations, *The Journal of Chemical Physics* **152**, 0007045 (2020).
- [33] SpaceX — spacex.com, <https://www.spacex.com/vehicles/falcon-heavy> (2024).
- [34] SpaceX Falcon 9 rocket launches Starlink satellites on record 21st flight (video) — space.com, <https://www.space.com/spacex-starlink-21st-falcon-9-launch-may-2024> (2024).
- [35] W. Pang, C. Deng, H. Li, L. T. DeLuca, D. Ouyang, H. Xu, and X. Fan, Effect of nano-sized energetic materials (nems) on the performance of solid propellants: A review, *Nanomaterials* **12**, 133 (2021).
- [36] S. Gharibian and F. Le Gall, Dequantizing the quantum singular value transformation: hardness and applications to quantum chemistry and the quantum pcp conjecture, in *Proceedings of the 54th Annual ACM SIGACT Symposium on Theory of Computing*, STOC '22 (ACM, 2022).
- [37] J.-L. Chen and W.-P. Hu, Theoretical prediction on the thermal stability of cyclic ozone and strong oxygen tunneling, *Journal of the American Chemical Society* **133**, 16045 (2011).
- [38] J. L. Bao and D. G. Truhlar, Variational transition state theory: theoretical framework and recent developments, *Chemical Society Reviews* **46**, 7548 (2017).
- [39] W.-P. Hu, Y.-P. Liu, and D. G. Truhlar, Variational transition-state theory and semiclassical tunnelling calculations with interpolated corrections: a new approach to interfacing electronic structure theory and dynamics for organic reactions, *Journal of the Chemical Society, Faraday Transactions* **90**, 1715 (1994).
- [40] H. Jónsson, G. Mills, and K. W. Jacobsen, in *Classical and Quantum Dynamics in Condensed Phase Systems*, edited by B. J. Berne, G. Cicotti, and D. F. Coker (World Scientific, 1998).
- [41] G. Henkelman and H. Jónsson, A climbing image nudged elastic band method for finding saddle points and minimum energy paths, *The Journal of Chemical Physics* **113**, 9901 (2000).
- [42] G. Henkelman and H. Jónsson, Improved tangent estimate in the nudged elastic band method for finding minimum energy paths and saddle points, *The Journal of Chemical Physics* **113**, 9978 (2000).
- [43] S. Grimme, C. Bannwarth, and P. Shushkov, A Robust and Accurate Tight-Binding Quantum Chemical Method for Structures, Vibrational Frequencies, and Noncovalent Interactions of Large Molecular Systems Parametrized for All spd-Block Elements (Z = 1-86), *J. Chem. Theory. Comput.* **13**, 1989 (2017).
- [44] A. Ricci and G. Ciccotti, Algorithms for Brownian dynamics, *Molecular Physics* **101**, 1927 (2003).
- [45] T. D. Kuhne, M. Krack, F. R. Mohamed, and M. Parrinello, Efficient and accurate Car–Parrinello–like approach to Born–Oppenheimer molecular dynamics, *Physical Review Letters* **98**, 066401 (2007).
- [46] A. Onuki, Theory of applying heat flow from thermostatted boundary walls: Dissipative and local–equilibrium responses and fluctuation theorems, *The Journal of Chemical Physics* **151**, 134118 (2019).
- [47] D. S. Sabirov, R. G. Bulgakov, and S. L. Khursan, Reactivity of carbonyl oxides generated by the ozonolysis of c60 and c70 fullerenes: a chemiluminescence study and quantum-topological analysis, *Mendeleev Communications* **20**, 231 (2010).
- [48] D. Sabirov, S. Khursan, and R. Bulgakov, Ozone addition to C60 and C70 fullerenes: A DFT study, *Journal of Molecular Graphics and Modelling* **27**, 124 (2008).
- [49] S. Fomichev, K. Hejazi, M. S. Zini, M. Kiser, J. F. Morales, P. A. M. Casares, A. Delgado, J. Huh, A.-C. Voigt, J. E. Mueller, and J. M. Arrazola, Initial state preparation for quantum chemistry on quantum computers (2023), [arXiv:2310.18410 \[quant-ph\]](https://arxiv.org/abs/2310.18410).
- [50] D. Malz, G. Styliaris, Z.-Y. Wei, and J. I. Cirac, Preparation of Matrix Product States with Log–Depth Quantum Circuits, *Physical Review Letters* **132**, 040404 (2024).
- [51] S. Lee, J. Lee, H. Zhai, Y. Tong, A. M. Dalzell, A. Kumar, P. Helms, J. Gray, Z.-H. Cui, W. Liu, M. Kastoryano, R. Babbush, J. Preskill, D. R. Reichman, E. T. Campbell, E. F. Valeev, L. Lin, and G. K.-L. Chan, Evaluating the evidence for exponential quantum advantage in ground-state quantum chemistry, *Nature Communications* **14**, 1 (2023).
- [52] A. Chapman and S. T. Flammia, Characterization of solvable spin models via graph invariants, *Quantum* **4**, 278 (2020).
- [53] S. J. Elman, A. Chapman, and S. T. Flammia, Free fermions behind the disguise, *Communications in Mathematical Physics* **388**, 969 (2021).
- [54] A. Chapman, S. J. Elman, and R. L. Mann, A unified graph-theoretic framework for free-fermion solvability, arXiv e-prints (2023), [arXiv:2305.15625](https://arxiv.org/abs/2305.15625).
- [55] A. Y. Kitaev, Quantum measurements and the abelian stabilizer problem, arXiv e-prints (1995), [arXiv:quant-ph/9511026](https://arxiv.org/abs/quant-ph/9511026).
- [56] D. W. Berry, M. Kieferová, A. Scherer, Y. R. Sanders, G. H. Low, N. Wiebe, C. Gidney, and R. Babbush, Improved techniques for preparing eigenstates of fermionic Hamiltonians, *NPJ Quantum Inf.* **4**, 22 (2018).

- [57] D. Poulin, A. Kitaev, D. S. Steiger, M. B. Hastings, and M. Troyer, Quantum Algorithm for Spectral Measurement with a Lower Gate Count, *Physical Review Letters* **121**, 010501 (2018).
- [58] R. Babbush, C. Gidney, D. W. Berry, N. Wiebe, J. McClean, A. Paler, A. Fowler, and H. Neven, Encoding electronic spectra in quantum circuits with linear T complexity, *Physical Review X* **8**, 041015 (2018).
- [59] A. M. Childs and N. Wiebe, Hamiltonian simulation using linear combinations of unitary operations, *Quantum Inf. Comput.* **12**, 901 (2012).
- [60] D. W. Berry, A. M. Childs, R. Cleve, R. Kothari, and R. D. Somma, Simulating Hamiltonian Dynamics with a Truncated Taylor Series, *Physical Review Letters* **114**, 090502 (2015).
- [61] W. J. Hehre, R. F. Stewart, and J. A. Pople, Self-consistent molecular-orbital methods. i. use of gaussian expansions of slater-type atomic orbitals, *The Journal of Chemical Physics* **51**, 2657 (1969).
- [62] T. H. Dunning Jr, Gaussian basis sets for use in correlated molecular calculations. i. the atoms boron through neon and hydrogen, *The Journal of Chemical Physics* **90**, 1007 (1989).
- [63] E. R. Sayfutyarova, Q. Sun, G. K.-L. Chan, and G. Knizia, Automated construction of molecular active spaces from atomic valence orbitals, *Journal of Chemical Theory and Computation* **13**, 4063 (2017).
- [64] Q. Sun, T. C. Berkelbach, N. S. Blunt, G. H. Booth, S. Guo, Z. Li, J. Liu, J. D. McClain, E. R. Sayfutyarova, S. Sharma, *et al.*, PySCF: the Python-based simulations of chemistry framework, *Wiley Interdisciplinary Reviews: Computational Molecular Science* **8**, e1340 (2018).
- [65] V. von Burg, G. H. Low, T. Häner, D. S. Steiger, M. Reiher, M. Roetteler, and M. Troyer, Quantum computing enhanced computational catalysis, *Physical Review Research* **3**, 033055 (2021).
- [66] W. van Dam, M. Mykhailova, and M. Soeken, Using Azure Quantum Resource Estimator for Assessing Performance of Fault Tolerant Quantum Computation, in *Proceedings of the SC '23 Workshops of The International Conference on High Performance Computing, Network, Storage, and Analysis*, SC-W '23 (Association for Computing Machinery, New York, NY, USA, 2023) pp. 1414–1419.
- [67] M. E. Beverland, P. Murali, M. Troyer, K. M. Svore, T. Hoefer, V. Kliuchnikov, G. H. Low, M. Soeken, A. Sundaram, and A. Vaschillo, Assessing requirements to scale to practical quantum advantage (2022), [arXiv:2211.07629](https://arxiv.org/abs/2211.07629).
- [68] K. Obenland, J. Elenewski, K. J. Morrell, R. S. Neumann, A. Kurlej, R. Rood, J. Blue, J. Belarge, B. Rempfer, and P. Kuklinski, [isi-usc-edu/pyliqtr:](https://isi-usc-edu/pyliqtr/) Release 1.1.1 (2024).
- [69] Microsoft, [Azure quantum resource estimation samples](https://www.microsoft.com/en-us/quantum/resource-estimation-samples), [Online] (2024).
- [70] A. G. Fowler, M. Mariantoni, J. M. Martinis, and A. N. Cleland, Surface codes: Towards practical large-scale quantum computation, *Physical Review A* **86**, 032324 (2012).
- [71] D. Horsman, A. G. Fowler, S. Devitt, and R. Van Meter, Surface code quantum computing by lattice surgery, *New Journal of Physics* **14**, 123011 (2012).
- [72] D. Litinski, A Game of Surface Codes, *Quantum* **3**, 128 (2019).
- [73] S. Bravyi and A. Kitaev, Universal quantum computation with ideal Clifford gates and noisy ancillas, *Physical Review A* **71**, 022316 (2005).
- [74] E. Aprà, E. J. Bylaska, W. A. de Jong, N. Govind, K. Kowalski, T. P. Straatsma, M. Valiev, H. J. J. van Dam, Y. Alexeev, J. Anchell, V. Anisimov, F. W. Aquino, R. Atta-Fynn, J. Autschbach, N. P. Bauman, J. C. Becca, D. E. Bernholdt, K. Bhaskaran-Nair, S. Bogatko, P. Borowski, J. Boschen, J. Brabec, A. Bruner, E. Cauët, Y. Chen, G. N. Chuev, C. J. Cramer, J. Daily, M. J. O. Deegan, T. H. Dunning, M. Dupuis, K. G. Dyall, G. I. Fann, S. A. Fischer, A. Fonari, H. Früchtl, L. Gagliardi, J. Garza, N. Gawande, S. Ghosh, K. Glaesemann, A. W. Götz, J. Hammond, V. Helms, E. D. Hermes, K. Hirao, S. Hirata, M. Jacquelin, L. Jensen, B. G. Johnson, H. Jónsson, R. A. Kendall, M. Klemm, R. Kobayashi, V. Konkov, S. Krishnamoorthy, M. Krishnan, Z. Lin, R. D. Lins, R. J. Littlefield, A. J. Logsdail, K. Lopata, W. Ma, A. V. Marenich, J. Martin del Campo, D. Mejia-Rodriguez, J. E. Moore, J. M. Mullin, T. Nakajima, D. R. Nascimento, J. A. Nichols, P. J. Nichols, J. Nieplocha, A. Otero-de-la Roza, B. Palmer, A. Panyala, T. Pirojsirikul, B. Peng, R. Peverati, J. Pittner, L. Pollack, R. M. Richard, P. Sadayappan, G. C. Schatz, W. A. Shelton, D. W. Silverstein, D. M. A. Smith, T. A. Soares, D. Song, M. Swart, H. L. Taylor, G. S. Thomas, V. Tippuraju, D. G. Truhlar, K. Tsemekhman, T. Van Voorhis, Á. Vázquez-Mayagoitia, P. Verma, O. Villa, A. Vishnu, K. D. Vogiatzis, D. Wang, J. H. Weare, M. J. Williamson, T. L. Windus, K. Woliński, A. T. Wong, Q. Wu, C. Yang, Q. Yu, M. Zacharias, Z. Zhang, Y. Zhao, and R. J. Harrison, NWChem: Past, present, and future, *The Journal of Chemical Physics* **152**, 184102 (2020).
- [75] M. Otten, B. Kang, D. Fedorov, J.-H. Lee, A. Benali, S. Habib, S. K. Gray, and Y. Alexeev, Qrechem: quantum resource estimation software for chemistry applications, *Frontiers in Quantum Science and Technology* **2**, 1232624 (2023).
- [76] M. Reiher, N. Wiebe, K. M. Svore, D. Wecker, and M. Troyer, Elucidating reaction mechanisms on quantum computers, *Proceedings of the National Academy of Sciences* **114**, 7555 (2017).
- [77] J. J. Goings, A. White, J. Lee, C. S. Tautermann, M. Degroote, C. Gidney, T. Shiozaki, R. Babbush, and N. C. Rubin, Reliably assessing the electronic structure of cytochrome p450 on today's classical computers and tomorrow's quantum computers, *Proceedings of the National Academy of Sciences* **119**, e2203533119 (2022).
- [78] Y. Su, D. W. Berry, N. Wiebe, N. Rubin, and R. Babbush, Fault-tolerant quantum simulations of chemistry in First Quantization, *PRX Quantum* **2**, 040332 (2021).
- [79] J. Cohn, M. Motta, and R. M. Parrish, Quantum Filter Diagonalization with Compressed Double-Factorized Hamiltonians, *PRX Quantum* **2**, 040352 (2021).
- [80] R. J. Buenker and S. D. Peyerimhoff, Individualized configuration selection in ci calculations with subsequent energy extrapolation, *Theoretica Chimica Acta* **35**, 33 (1974).

- [81] R. J. Buenker, S. D. Peyerimhoff, and W. Butscher, Applicability of the multi-reference double-excitation ci (mrd-ci) method to the calculation of electronic wavefunctions and comparison with related techniques, *Molecular Physics* **35**, 771 (1978).
- [82] H.-J. Werner and P. J. Knowles, An efficient internally contracted multiconfiguration–reference configuration interaction method, *The Journal of Chemical Physics* **89**, 5803 (1988).
- [83] C.-H. Huang, R.-M. You, P.-Y. Lian, and W.-P. Hu, Improved interpolated correction schemes for dual-level direct dynamics calculation, *The Journal of Physical Chemistry A* **104**, 7200 (2000).

Supplementary Information

Appendix A: Complete Workflow for Fullerene-assisted Synthesis of Cyclic Isomer of Ozone

1. Formulation and objectives

We consider the computational cost of applying a computational approach for determining the thermal stability of a single isolated cyclic ozone molecule developed in Ref. [37] to the cyclic ozone molecule within the endofullerene ($x\text{O}_3, y\text{O}_2\text{@C}_n$). This approach relies on variational transition state theory (VTST). At a high level, VTST requires that we can compute the Born-Oppenheimer (BO) energy for specific points along the reaction pathway [38, 39]. Vibrational frequencies may also be required and come at a higher computational cost. Additionally, VTST requires we have a lower level of theory calculation that captures the qualitative shape of the potential energy surface (PES) along the reaction coordinate.

Mathematically, for a one dimensional tunnelling model, we first aim to interpolate the BO energy $V(s)$ along the minimum energy pathway (MEP) with reaction coordinate $s \in [-1, 1]$ where $V(s = -1), V(s = +1), V(s = 0)$ are the BO energies at the reactant, product, and saddle point geometries [38]. In this case $s = -1$ is cyclic ozone, $s = +1$ is bent ozone, and $s = 0$ is a transition state between the two. Let $V_{\text{HL}}(s)$ be the high accuracy PES i.e., $V_{\text{HL}}(s) = V(s)$. Let $V_{\text{LL}}(s)$ be the lower accuracy PES (e.g., DFT). Then the correction function $\Delta V = V_{\text{HL}}(s) - V_{\text{LL}}(s)$ is approximated by an Eckart potential, shown in Fig. 11 of the form

$$\Delta V(s) = \frac{Ay(s)}{1 + y(s)} + \frac{By(s)}{(1 + y(s))^2} + C \quad (\text{A1})$$

where

$$y(s) = \exp((s - s_0)/L), \quad (\text{A2})$$

$$A = \Delta V(+1) - \Delta V(-1), \quad (\text{A3})$$

$$C = \Delta V(-1), \quad (\text{A4})$$

$$B = (2\Delta V(0) - A - 2C) \pm 2[(\Delta V(0) - C)(\Delta V(0) - A - C)]^{1/2}, \quad (\text{A5})$$

and

$$s_0 = -L \ln((A + B)/(B - A)). \quad (\text{A6})$$

Using the SIL-1 technique [83] we need one additional high accuracy point on the PES that is on the reactant side of the MEP $s = s_{1/2} \in [-1, 0)$ and not too close to the saddle point $s = 0$. Using this additional point, the range parameter L is chosen such that

$$V_{\text{LL}}(s_{1/2}) + \Delta V(s_{1/2}; L) = (V_{\text{HL}}(s_{1/2}) - V_{\text{HL}}(-1))/2. \quad (\text{A7})$$

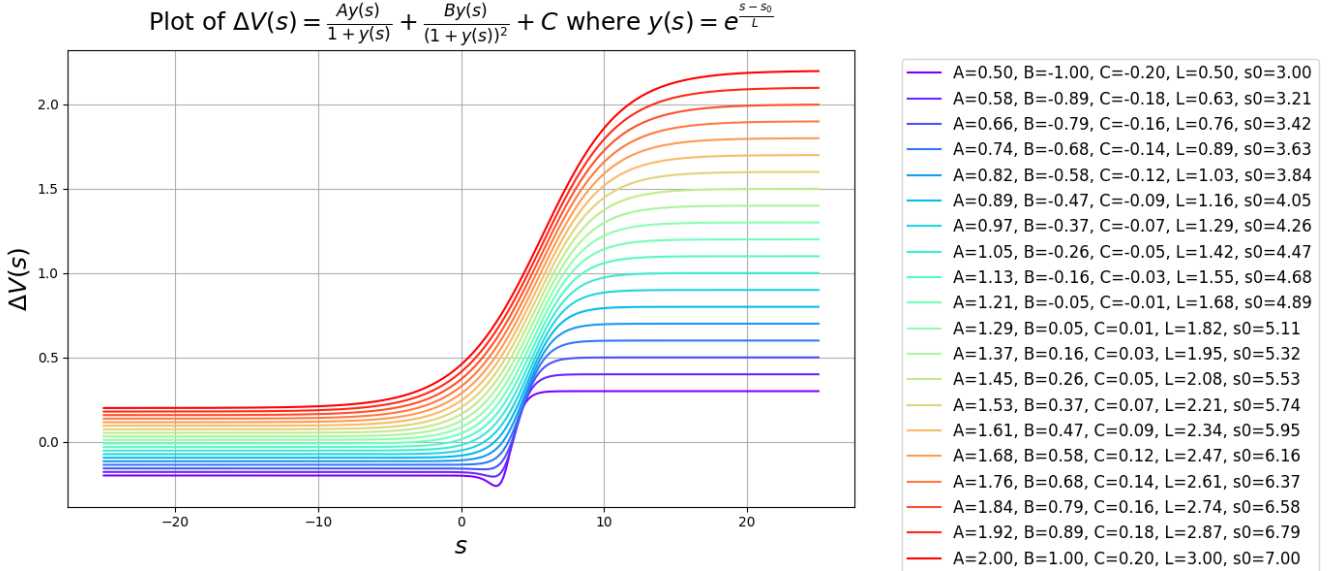


FIG. 11. Eckart Potentials for various choices for parameters A, B, C, L, s_0 for $s \in [-25, 25]$.

Thus, all the information we require from our high level of theory calculations (e.g., via quantum computation) are the BO energies at $s = 0, \pm 1, s_{1/2}$. Additionally, we may require high accuracy in our estimation of vibrational frequencies which we can obtain using a similar interpolation procedure for the vibrational frequencies correction functions $\Delta\omega_m(s) = \omega_{m,HL}(s) - \omega_{m,LL}(s)$ [39] where $\omega_m(s)$ are the vibrational frequencies computed from the eigenvalues of the Hessian $H \in \mathbb{R}^{3N \times 3N}$ along the reaction coordinate s

$$H_{ij}(s) = \left. \frac{\partial^2 V(\mathbf{R})}{\partial R_i \partial R_j} \right|_{\mathbf{R}=\mathbf{R}(s)}. \quad (\text{A8})$$

In order to obtain high accuracy BO energies at $s = 0, \pm 1, s_{1/2}$, we need high quality molecular geometries. The previous VTST study of a single ozone molecule used multi-reference methods to optimize molecular geometries in addition to BO energies at $s = 0, \pm 1, s_{1/2}$ [37]. This step likely requires the estimation of atomic forces on 3 oxygen atoms at a high level of theory.

Once we have fit $\Delta V(s)$ to the isomerization reaction pathway, we compute the generalized rate constant along the reaction pathway $k(s, T)$ where T is temperature as

$$k(s, T) = \frac{k_B T}{h} \frac{Q^{GT}(T, s)}{Q^R(T)} \exp\left(-\frac{V_{HL}(s)}{k_B T}\right) \quad (\text{A9})$$

where $Q^{GT}(T, s)$ is the partition function of the generalized transition state (GT), that is, at a given geometry s along the reaction pathway $s \in [-1, 1]$. $Q^R(T)$ is the partition function at the reactant (cyclic ozone) and h is Planck's constant. VTST then estimates the true reaction rate constant $k(T)$ as

$$k(T) = \kappa(T) \times \min_s k(s, T) \quad (\text{A10})$$

Following Ref. [37], the transmission coefficient $\kappa(T)$ can be obtained using the microcanonical optimized multidimensional tunneling (μ OMT) correction evaluated at continuous energy levels and at quantized reactant states (QRST) along the reaction pathway.

In summary, this workflow requires us to compute the following quantities at varying levels of chemical theory:

- Low-level BO energies $V_{LL}(s)$ at $s \in [-1, 1]$
- High-level BO energies $V_{HL}(s)$ at $s = 0, \pm 1, s_{1/2}$

- Low-level Born-Oppenheimer atomic forces \mathbf{F}_I^{BO}
- Low-level vib. frequencies $\omega_{m,LL}(s)$ at $s \in [-1, 1]$
- If high accuracy frequencies are required, high-level vib. frequencies $\omega_{m,HL}(s)$ at $s = 0, \pm 1$

An important base case for studying these ozone systems is to consider the energetics of a single isolated ozone molecule. Several studies [13, 15, 37] have investigated the potential energy landscape of ozone and computed geometries of product, reactant, and intermediate transition states involved in the isomerization of cyclic ozone to bent ozone. In Table II the energetics of ozone are computed using different multi-reference methods is reported. We consider the source of truth to be Semistochastic Heat Bath Configuration Interaction [15] which is a selected-CI algorithm that can obtain FCI-level energies for ozone. In Table III, the optimized geometries obtained using various classical algorithms which can serve as a starting point for computing intermediate geometries for the isomerization of ozone within a fullerene cage.

Method	Open Min.	TS	Ring Min.	CP1	CP2
MRCISD+Q(18,12)/aug-cc-pVTZ ^a	0.00	2.42	1.33	2.19	1.64
MRCISD+Q(18,12)/aug-cc-pVQZ ^a	0.00	2.48	1.36	2.28	1.72
CASSCF(18,12)/aug-cc-pVTZ ^a	0.00	2.30	1.32	2.13	1.61
CASSCF(18,12)/cc-pVTZ ^b	0.00	2.29	1.30		
CASSCF(18,12)/cc-pVQZ ^b	0.00	2.32	1.33		
extrapolated SHCI/cc-pVTZ ^c	0.00	2.41	1.30		

TABLE II. Born-Oppenheimer 1^1A_1 energies (eV) relative to bent (open) ozone ^a Ref. [37], ^b ref. [13] , ^c Ref. [15]

Method	Open	Cyclic	TS	CP1	CP2
	$R_{OO} \angle$				
MRCISD+Q(18,12)/aug-cc-pVTZ ^a	1.291 116.7	1.457 60.0	1.427 83.8	1.416 80.3	1.406 89.2
CASSCF(18,12)/aug-cc-pVTZ ^a	1.282 116.7	1.449 60.0	1.410 84.0	1.416 79.7	1.401 89.6
CASSCF(18,12)/cc-pVTZ ^b	1.292 116.5	1.466 60.0	1.424 84.1		
CASSCF(18,12)/cc-pVQZ ^b	1.288 116.6	1.465 59.9	1.428 84.0		
exp ^a	1.273 116.8				

TABLE III. Optimized isolated ozone geometries where R_{OO} denotes bond length and \angle denote bond angle ^a ref. [37], ^b ref. [13]

2. Inputs

At a high level, the input to the computational workflow described herein is the chemical composition of the endofullerene we wish to investigate, for example $(5O_3, 4O_2)@C_{180}$. This chemical composition must then be converted into an initial molecular geometry typically specified by .xyz files. There are additional inputs are required by subroutines in the workflow. Specifically, the quantum portion of the workflow requires the appropriate size of the supercell, accuracy thresholds, the calculated Hartree-Fock state or some multi-reference state that can be used as the initial state for quantum phase estimation. On the classical side, it is important to choose appropriate an DFT functional and basis set for describing the low-level PES of the oxygen-encapsulating endofullerene. In this work we consider the PBE functional and cc-pVTZ basis set.

3. Outputs

The ultimate goal of the workflow is to determine the stability of cyclic ozone within a given oxygen-containing endofullerene. This workflow considers stability with respect to the cage's ability to hold the oxygen as well as the rate of isomerization for ozones in the cage. We seek the oxygen-containing endofullerene that makes the isomerization rate constant as small as possible. The workflow is designed to allow for sampling multiple different configurations of ozone within the fullerene cage. For each sampled geometry, we consider computing the isomerization rate for several ozone molecules. For small endofullerenes, we could consider the isomerization rate for every single ozone molecule for each sampled initial geometry. However for larger endofullerenes, such as $(116 O_3)@C_{720}$, this may be

too computationally intensive and we may need to resort to sampling a subset of ozone molecules to compute the isomerization rate for.

4. Workflow Pseudocode

The pseudocode provided here reflects the computational workflow depicted in Fig. 4. Within this pseudocode, steps of the algorithm are classified by the quantum or classical subroutines required to carry that step out. Density functional theory (DFT) is a classical algorithm, whereas quantum phase estimation (QPE) is a quantum algorithm. Overall, this workflow estimates the stability of cyclic ozone within the fullerene C_n in the presence of other forms of oxygen such as O_2 or the bent form O_3 . Stability is quantified by a rate constant $k(T)$ at a given temperature T , a smaller rate constant indicates that the stability of ozone against isomerization into bent ozone.

Input: Chemical composition $(xO_3, yO_2)@C_n$

Output: Isomerization Rate Constants $k(T)$

```

1  $N_{\text{geos}} \leftarrow$  number of geometries we wish to consider
2  $x \leftarrow$  number of cyclic ozone molecules to compute isomerization rate in  $(xO_3, yO_2)@C_n$ 
3 for  $i = 1, \dots, N_{\text{geos}}$  do
4   Generate initial geometry (XTB, langevin dynamics), (DFT, geometric optimization)
5   Compute formation energy  $\Delta E$  (DFT, total energy) [9]
6   Compute bond elongation  $\epsilon$  and internal pressure  $P(\epsilon)$  (DFT,  $n$  atomic forces) [9]
7   for  $j = 1, \dots, x$  do
8     Run CI-NEB to find reaction pathway (DFT, geometric optimization)
9     Compute "high-level" energies  $V_{HL}(s)$  at  $s = 0, \pm 1, s_{1/2}$  point (quantum computer, quantum phase estimation)
10    Compute vibrational frequencies  $\omega_{m,LL}(s)$  for  $s = 0, \pm 1$  (DFT, Hessian diagonalization)
11    Compute transmission coefficient  $\kappa(T)$  with microcanonical optimized multidimensional tunneling correction
12      [37]
12    Compute rate constant  $k(T) = \kappa(T) \times \min_s k(s, T)$  (DFT, compute  $V(s) = V_{LL}(s) + \Delta V(s)$ )

```
